Compressed Air Energy Storage with Liquid Air Capacity Extension

Bharath Kantharaj[1], Seamus Garvey & Andrew Pimm

Division of Materials, Mechanics and Structures, Faculty of Mechanical Engineering, University of Nottingham, Nottingham, NG7 2RD, United Kingdom

ABSTRACT

As renewable electricity generation capacity increases, energy storage will be required at larger scales. Compressed air energy storage (CAES) at large scales, with effective management of heat, is recognised to have potential to provide affordable grid-scale energy storage. Where suitable geologies are unavailable, compressed air could be stored in pressurised steel tanks above ground, but this would incur significant storage costs. Liquid air energy storage (LAES), on the other hand, does not need a pressurised storage vessel, can be located almost anywhere, has a relatively large volumetric exergy density at ambient pressure, and has relatively low marginal cost of energy storage capacity even at modest scales. However, it has lower roundtrip efficiency than compressed air energy storage technologies. This paper carries out thermodynamic analyses for an energy storage installation comprising a compressed air component supplemented with a liquid air store, and additional machinery to transform between gaseous air at ambient temperature and high pressure, and liquid air at ambient pressure. A roundtrip efficiency of 42% is obtained for the conversion of compressed air at 50bar to liquid air, and back. The proposed system is more economical than pure LAES and more economical than a pure CAES installation if the storage duration is sufficiently long and if the high-pressure air store cannot exploit some large-scale geological feature.

Keywords: Energy storage; Compressed air energy storage; Liquid air energy storage; Multistream plate-fin heat exchanger; Exergy.

[1] Corresponding author
E-mail: Bharath.Kantharaj@nottingham.ac.uk; Tel.: +44 115 846 7683.

NOMENCLATURE

A	Total heat transfer area (m^2)
A_f	Secondary (fin) heat transfer area (m^2)
A_o	Free-flow area (m^2)
A_p	Primary heat transfer area (m^2)
A_w	Area of the wall (m^2)
$\dot{B}$	Flow exergy of a fluid (W)
C	Compressor
C_p	Specific heat capacity at constant pressure (J/kgK)
C_v	Specific heat capacity at constant volume (J/kgK)
D	Diameter of the outer shell (m)
D_h	Hydraulic diameter (m)
E	Expander
G	Mass flow velocity (kg/m^2s)
J	Colburn factor
L_{eff}	Effective total length of the fin (m)
L_f	Effective fin length (m)
L_1	Length of the heat exchanger (m)
L_2	Width of the heat exchanger (m)
N	Number of stages in an *MEHXp*/*MCHXp* unit
N_f	Number of fins
N_{off}	Number of offset fins
N_p	Number of passages
N_{SP}	Number of separating plates
P	Pressure (Pa)
P_w	Wetted parameter (m)
Pr	Prandtl number
$\dot{Q}$	Heat content of a stream (W)

Re	Reynolds number
R_p	Pressure ratio across one stage of a compressor/an expander
R_w	Wall resistance (K/W)
T	Temperature (K)
UA	Global conductance (W/K)
V	Vent to the atmosphere
$\dot{W}_{net}$	Rate of net work into/out of the system (W)
a	Plate thickness (m)
b	Fin height (m)
d	Diameter of the inner tube (m)
g	Acceleration due to gravity (m/s^2)
h	Specific enthalpy (J/kg)
k	Thermal conductivity (W/mK)
l	Fin length for conduction (m)
m	Fin parameter (m^{-1})
$\dot{m}$	Mass flow rate (kg/s)
p_f	Fin pitch (m)
s	Specific entropy (J/kgK)
t_w	Wall thickness (m)
x	Liquid fraction
y	Vapour fraction
AH	After-heater
$Amb.$	Ambient conditions
PC	Pre-cooler
$MCHXp$	Multistage compression with heat exchangers in parallel
$MEHXp$	Multistage expansion with heat exchangers in parallel

GREEK

ΔH_{2p}	Latent heat associated with phase change of air (J/kg)

ΔT	Temperature difference between the hot and cold fluids (K)
ΔT_{2p}	Film to wall temperature difference during phase change of air (K)
α	Heat transfer coefficient (W/m^{2}K)
γ	Ratio of specific heat
δ	Fin thickness (m)
ε	Heat exchanger effectiveness (%)
ξ	Interrupted fin length in the fluid flow direction (m)
η	Efficiency (%)
η_f	Fin efficiency (%)
η_o	Heat transfer surface effectiveness (%)
μ	Viscosity (Ns/m^2)
ρ	Density (kg/m^3)

SUBSCRIPTS/SUPERCRIPTS

CA	Compressed air
F	Forward conversion process
LA	Liquid air
R	Reverse conversion process
air	Air (real gas properties)
$cold$	Cold stream in a heat exchanger unit
$comp$	Compressor
$elec, CA$	Electricity to compressed air (or vice versa)
$elec, LA$	Electricity to liquid air
ex	Exergy
exp	Expander
f	Fin
hot	Hot stream in a heat exchanger unit
i	Inner
iso	Isothermal

l	Liquid
m	Mean
o	Outer
pri	Primary air
ref	Refrigerant (ideal gas properties)
s	Isentropic process
sec	Secondary air
w	Wall
$2p$	Two-phase

1. INTRODUCTION

In 2012, wind power accounted for 39% of renewable power capacity added worldwide, followed by 26% each for solar PV and hydropower [1]. The capacities of the major renewable energy sources are expected to increase in the future. Increasing renewable energy penetration, especially wind, is crucial for decarbonising the grid. As an example, the UK aims to reduce greenhouse gas emissions by 80%, based on 1990 levels, by 2050 [2]. But renewable energy sources, for example wind, are intermittent, and the associated uncertainty with electricity generation from such sources can lead to grid stability issues [3, 4]. It is here that bulk energy storage technologies, such as Pumped Hydro Storage (PHS) or Compressed Air Energy Storage (CAES), are expected to play a key role, by offering services primarily in energy management (load levelling and following, power balancing, peak shaving, etc.) [5].

The case for CAES has been made by many [6, 7, 8, 9, 10, 11] and need not be rehearsed again here. CAES at large scales has historically been used as a "stand by" power source for smoothing applications. For CAES to be cost effective, it must be employed at large scales (e.g. underground salt caverns, aquifers), but geological constraints prevent widespread deployment of this variant of CAES technologies. An alternative is aboveground storage of compressed air in pressurised steel tanks, but it can incur significant storage costs (see section 2.1).

In the recent past, Liquid Air Energy Storage (LAES) has experienced a surge in interest [12] and has been considered a possible candidate for bulk storage of electrical energy, particularly in the UK [13]. Liquid air, unlike compressed air, has high energy density and can thus be compactly stored. LAES also has the strong advantage that it can be located almost anywhere. It does not need a pressurised vessel for storage, just a well-insulated container.

In this paper, we propose a novel hybrid energy storage system which comprises an aboveground compressed air storage tank supplemented with a liquid air storage tank. To the authors' knowledge, an energy storage system comprising both compressed air and liquid air storage technologies has not been proposed before. The system attempts to exploit the different characteristics of CAES and LAES, i.e., the relatively higher roundtrip efficiency of CAES, and low cost per unit of energy storage capacity of LAES. The system comprises a compressed air store of relatively lower energy storage capacity, a liquid air store of higher energy storage capacity (the efficiency of liquefaction plants depends strongly on their scale [14]), and machinery to transform between the two states of air. The low-frequency components of power are associated with large quantities of stored energy and are mainly handled by the conversion between liquid air and compressed air. The higher-frequency components of power are mainly handled by CAES alone. Thus, when electricity prices are low, and the compressed air tank is nearly full, electricity can still be drawn from the grid by converting some amount of compressed air into liquid air. Note that the first step in an air liquefaction process is the compression of ambient air. Conversely, when electricity prices are high, and the compressed air tank is nearly empty, electricity can still be exported to the grid by converting liquid air back to compressed air, and then to electricity. Here, the liquid air is stored at ambient pressure. This paper presents a detailed energy and exergy analysis of the proposed system, starting with the ideal configuration, followed by a possible practical arrangement. Economic analysis of hybrid energy storage systems [15] shows that such systems can have cost and performance advantages relative to either of the two individual storage technologies employed. The analysis performed here can serve as an initial guideline for the detailed design of a hybrid CAES-LAES plant.

The paper is organised as follows. In section 2, background information on CAES and LAES, including costs and performance of these technologies, is presented. In section 3, thermodynamic analysis of

the ideal hybrid energy storage system is carried out, followed by analysis of the practical cases. Finally, in section 4, some conclusions are drawn.

2. BACKGROUND

2.1. COSTS AND PERFORMANCE OF CAES

The working of a conventional CAES plant is similar to that of a gas turbine plant in principle, except that the compression and expansion processes are decoupled in time. During periods of low electricity price, electrical energy is withdrawn from the grid to generate compressed air, which is then cooled and stored in underground or aboveground containers. During times of peak demand, the compressed air is heated and expanded to produce work, and subsequently electricity. Around two-thirds of the power output by the expanders is consumed by the compressors in a gas turbine plant [16]. Thus, due to the decoupling, a CAES plant of similar size as a gas turbine plant provides significantly more output power. The power conversion machinery dominates the plant costs. Table 1 lists the costs for CAES systems collected from various sources, and is adapted from Ref. [17]. It is worth noting that the reference discharge time for large CAES technologies considered in Ref. [17] is 10 hours.

Table 1: Representative costs of CAES systems from various sources.

Source of estimate	Power related cost[2] ($/kW)	Storage cost[3] ($/kWh)
Schoenung and Hassenzahl (2003) (bulk storage)	425	3
Schoenung and Eyer (2008) (distributed generation/surface)	550	120
EPRI-DOE (2003) (salt mine 300 MWac)	270	1
EPRI-DOE (2003) (surface 10 MWac)	270	40
EPRI (2003) (salt/porous/hard rock/surface)	350 (all)	1/0.10/30/30
EPRI-D0E (2004) (salt/surface)	300	1.74/40

[2] Investment cost of the storage technology per unit of rated power output.
[3] Investment cost of the storage technology per unit of energy storage capacity.

At present, there are two large-scale CAES plants in operation. The first CAES plant was set up in Huntorf, Germany, in 1978 to function as a "minute reserve", i.e., to aid grid stability during times of sudden spikes in power demand. It operates between 46bar and 72bar, and at full capacity, it can provide 290MW of electricity for 4 hours [18]. The second CAES plant to be commissioned was set up in McIntosh, Alabama, in 1991. It operates between 45bar and 74bar, and provides 100MW of electricity for 26 hours at full capacity [19]. Both these plants store cool, compressed air in underground salt caverns. Per contra, CAES can also be operated isobarically. Here, the stores are maintained at a constant pressure irrespective of the total mass of air in storage. One example of an isobaric store employs a constant-volume air container from which water is displaced into an overhead reservoir whose level is largely insensitive to the degree of fill of the constant-volume container [20], and a second example involves using a flexible container to store air in deep sea [21]. In this article we assume isobaric operation of the compressed air store, but it is expected that the analyses could also be extended to an isochoric compressed air store.

Conventional CAES suffers from a major drawback, however, which is the burning of gas (a fossil fuel) in the generation phase. This is done to increase the power output of the plant, and it also prevents water vapour in the air from freezing during expansion. Thus, it is clear that for CAES to be a 'fuel-free' energy storage technology, heat has to be managed effectively – ideally the heat of compression should not be vented to atmosphere or allowed to leak through the walls of the storage tank, but be taken out of the air during or after the compression process and stored in dedicated thermal energy storage units, ready to later heat the air entering the expander.

Two main variants of conventional CAES have been proposed/are currently being investigated to circumvent this problem: Adiabatic-CAES (A-CAES), and Isothermal-CAES (I-CAES). The heat store in an A-CAES plant eliminates the need for a combustor, and is the central element of the plant. There are two ways of storing the heat of compression of air. One way is via direct contact between the airflow and the storage material, i.e., compressed air at high temperature is fed into a pressurised vessel containing the storage material, allowing for a large heat transfer area and thus low losses [22]. The main disadvantage is the high investment cost for the pressurised container. Moreover, compressors capable of handling high discharge temperatures (~600C) have to be built

[23], and the pressurised storage concept also requires high maintenance effort. The second method incorporates heat exchangers to move the heat between the compressed air and an ambient pressure thermal energy store. Although this does not need a pressure vessel, it requires heat exchangers with high effectiveness for the plant to be completely fuel free. The utility RWE, along with several other industrial partners, investigated the technical feasibility of this variant of CAES in "Project ADELE" [24]. More information on A-CAES, along with some recently proposed commercial concepts, can be found in Ref. [25, 26, 27].

I-CAES compresses and expands air near-isothermally. Here, the compressed air is stored in pressure vessels aboveground. A spray of water or an air-liquid mixture captures the heat of compression so that energy is stored in the form of cool air at high pressure and warm fluid at low pressure [28, 29]. During expansion, the mixture supplies heat back to the air which does work and generates electricity. For effective heat storage at larger scales of energy storage, the heat transfer area between the mixture and the compressed air must be very large, or the compression and expansion processes must be carried out in very many stages so that near-isothermal characteristics are achieved. The latter, however, has high investment costs associated with it.

2.2. COSTS AND PERFORMANCE OF LAES

If one removes sufficient heat from an isolated mass of air, it will liquefy. A simple air liquefaction cycle, the Linde-Hampson cycle, is shown in Fig. 1, and it employs the Joule-Thomson effect to produce liquid air. At ambient pressure, air becomes completely liquid at 78.9K. There has recently been a surge of interest in using liquid air as an "energy carrier", i.e. energy storage medium, as reported in [7, 12, 30], owing to its relatively high exergy density (competitive with existing battery technologies [7]) and its potential as a clean transport fuel [12]. Thus, LAES can be thought of as a thermo-electric storage device which stores energy as a temperature difference between two thermal reservoirs [31]. Generally, the LAES cycle involves [32]: (a) The charging of the liquid air store (i.e., the liquefaction process), with the liquid air then stored in a thermally insulated tank at near-ambient pressures; (b) The discharging of the liquid air store, where power is recovered by first pressurising the liquid air, then supplying thermal energy to the fluid, and subsequently expanding to generate

work output. This in turn drives a generator to feed electricity back to the grid; (c) 'Cold recycle', where cold thermal energy released during discharge is stored, and is used to minimise the liquefaction work during charging.

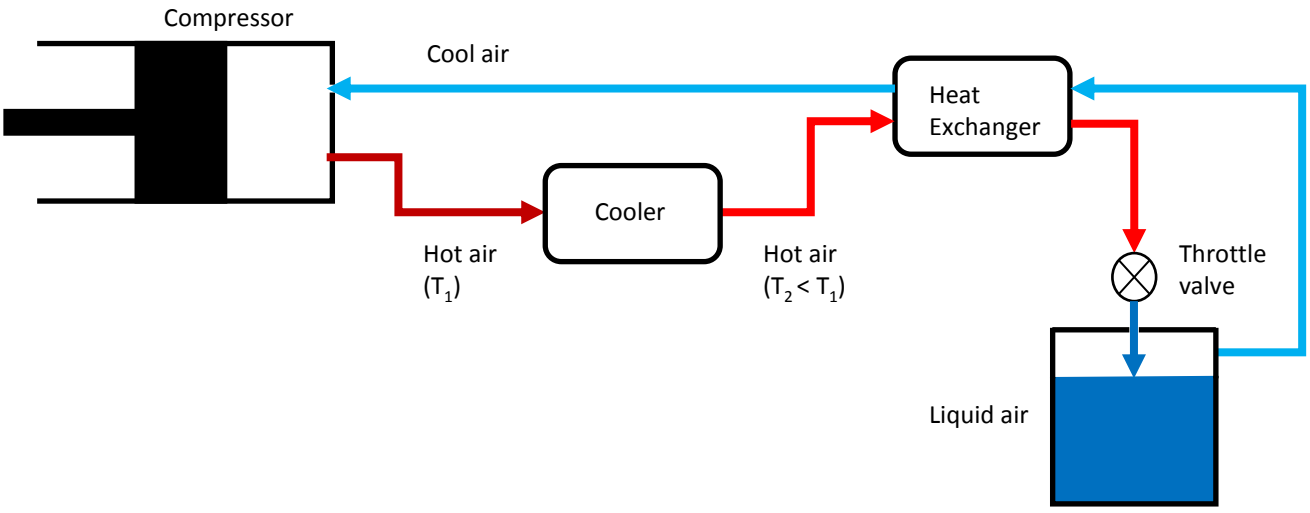

Figure 1: A simple air liquefaction cycle.

Interest in LAES goes back as far as 1977 when Smith [33] proposed a cycle using adiabatic compression and expansion, and reported an energy recovery efficiency of 72%. But this configuration required, most importantly, a regenerator which could withstand temperatures between -200C and 800C, pressures up to 100bar, and allow contact with both compressed air and liquid air. Ameel *et al*. [34] analyse a combined Rankine cycle with Linde liquefaction process, and report that 43% of the energy can be recovered from liquid air. Power recovery from cryogen via an indirect Rankine cycle is one of four major methods of extraction of cold exergy [35], with the other three being: (a) 'Direct expansion' cycle where pressurised cryogen is supplied with thermal energy from ambient or waste heat sources, and then expanded to extract work; (b) Indirect Brayton cycle where the cryogen cools down the gas at the inlet to a compressor, then the compressed gas is heated further before expansion. Here, the cryogen is used to minimise compression work; (c) Combination of either Rankine cycle with direct expansion or Brayton cycle with direct expansion.

More recently, a cryogenic energy storage system for electrical energy storage which uses liquid air/nitrogen as the energy carrier coupled with a natural gas-fuelled closed Brayton cycle was proposed [36]. The carbon dioxide produced in the cycle is captured as dry ice, and the roundtrip

efficiency is reported as 54%. Here, helium is used as the "blending gas" (it circulates within the system and is not consumed) to control the temperature of the natural gas after combustion in an oxygen rich environment, and before it enters a gas turbine. It is reported in Ref. [37] that for the system proposed in Ref. [36], capital costs dominate, and the air liquefaction unit accounts for a large part of the capital costs. The authors report that both the capital and peak electricity costs of the system are comparable with combined cycle gas turbine (CCGT) plant. The cost of the cryogenic tank depends, of course, on the capacity, and in terms of cost per rate of liquefaction, $30,000/(tonne/day) for a liquefaction plant with capacity of 500 tonne/day is suggested.

A demonstration LAES plant (350kW/2.5MWh) was built in 2008 in Slough, UK, and detailed analysis and results from the testing of this pilot plant can be found in Ref. [32].

3. THERMODYNAMIC ANALYSIS OF THE SERIES HYBRID ENERGY STORAGE SYSTEM BASED ON CAES AND LAES

The proposed hybrid energy storage system has a compressed air energy store of relatively low energy storage capacity and a liquid air energy store of higher energy storage capacity. All energy transactions with the grid will be carried out via the compressed air store and the liquid air store acts as *overflow* capacity (Fig. 2). When electricity prices are low and the compressed air energy store is nearly full, compressed air is converted via the system into liquid air and stored, so that more energy can be bought while prices are low. We will describe this process as *forward conversion* (high-pressure air $\rightarrow$ liquid air).

Conversely, when electricity prices are high, and the compressed air store is nearly empty, liquid air is converted back into compressed air, and the energy is then restored to the grid. We will describe this process as *reverse conversion* (liquid air $\rightarrow$ high-pressure air).

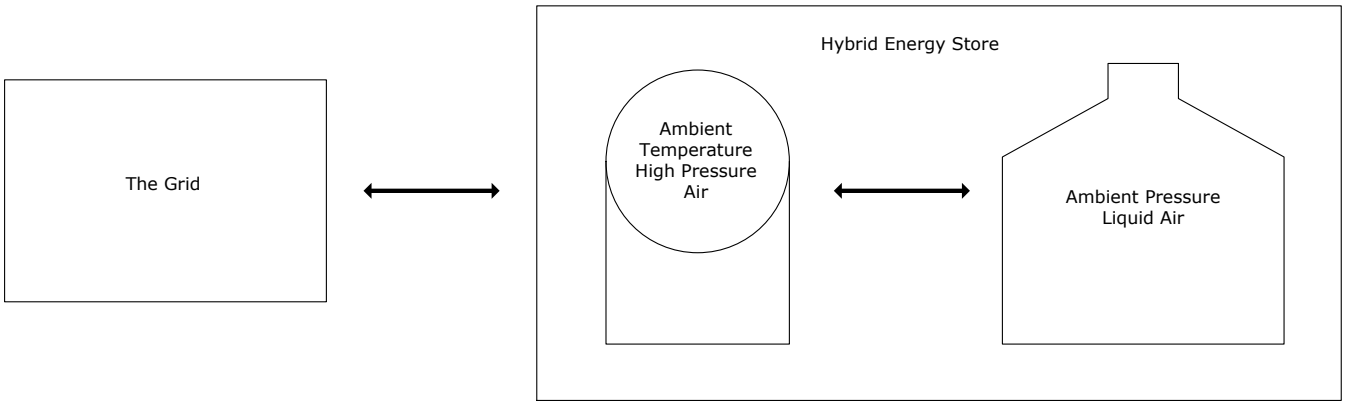

Figure 2: Energy flows for the hybrid energy storage system.

It should be noted that the term 'series' here means that all energy transactions with the grid will be via the compressed air energy store. The forward conversion process is an air liquefaction process, and the reverse process is the energy recovery process, where the recovery is accomplished by converting liquid air to compressed air and finally to electricity, rather than by expanding the pressurised, and subsequently heated, liquid air.

3.1. IDEAL, REVERSIBLE HYBRID ENERGY STORAGE SYSTEM

An analysis of the hybrid system must rely on *exergy* – the maximum work which can be obtained by allowing the system to come back into equilibrium with its ambient environment [38] – as it helps to locate irreversibilities in individual components. Neglecting kinetic and potential energy effects and assuming chemical reactions do not occur, flow exergy of a stream relative to ambient can be expressed as [39]:

$$\dot{B} = \dot{m}[h - h_o - T_o(s - s_o)] \quad (1)$$

Storing liquid air is storing exergy because as ambient heat is allowed back into that air, it will evaporate and do work. All pumped thermal electricity storage systems are implicitly exergy storage systems.

This section describes the configuration of an ideal reversible system and outlines an exergy analysis for this system. Based on this ideal system, considerable insight is gained into what features a practical system should have.

In the ideal (reversible) case for the hybrid energy storage system shown in below, there is no loss of exergy – all of the flow exergy of the compressed air is transformed to flow exergy of liquid air during the forward conversion. Similarly, all of the flow exergy of the liquid air is transformed back to flow exergy of ambient-temperature compressed air in the reverse conversion.

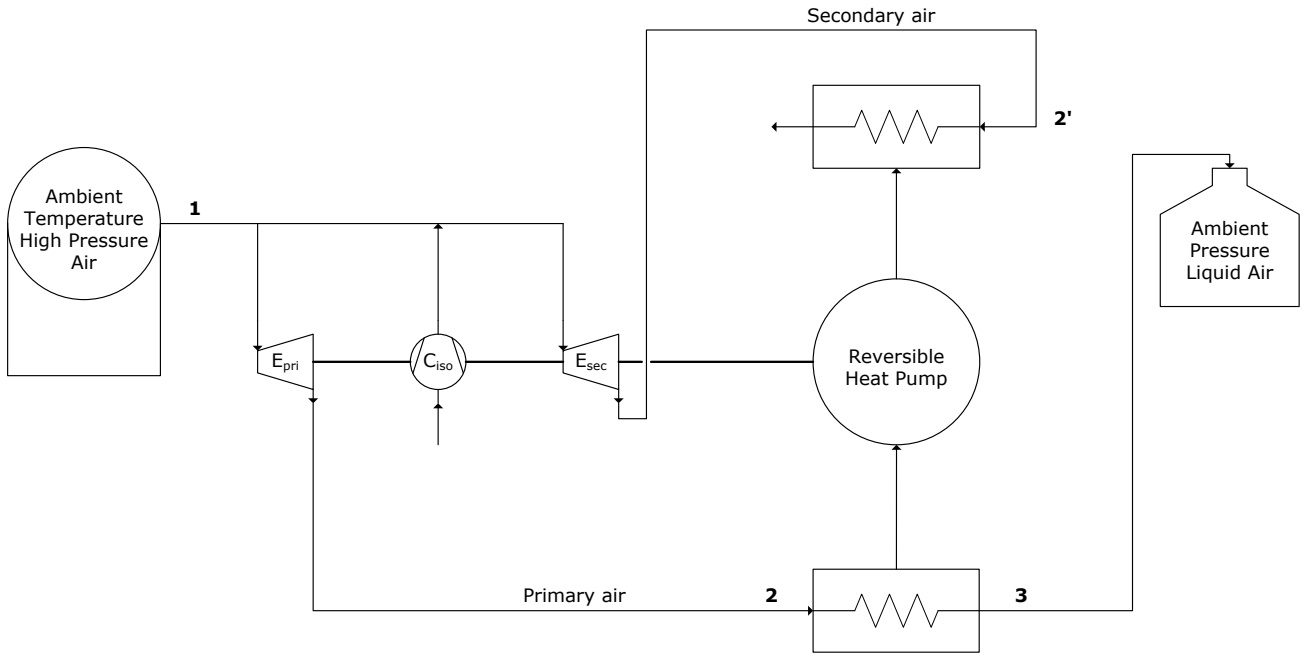

Figure 3: Schematic of the ideal (reversible) hybrid energy storage system.

For brevity in what follows, it is convenient to assign notation to some relevant temperatures:

T_1: Ambient temperature (290K is assumed for the cases studied here)

T_2: A temperature just above dew-point for atmospheric pressure air

T_3: A temperature just below bubble-point for atmospheric pressure liquid air

The forward conversion process is explained as follows. High-pressure air is drawn from the compressed air store in two different streams: *primary air* which is all ultimately converted into liquid form and *secondary air* whose exergy is exploited to provide additional cooling for the primary air. A straightforward exergy balance reveals the required mass-flow ratio between primary and secondary air. Taking ambient temperature to be 290K, and assuming that the high pressure air is stored at

50bar, 1kg of liquid air has the same flow exergy as ~2.2kg of compressed air. In that case, the ratio of mass flow rates of air in the primary and secondary streams is 1:1.2.

The primary air stream begins at high pressure and temperature T_1. This air is expanded isentropically to atmospheric pressure via the expander E_{pri} so that its temperature reduces to T_2. The primary air at point 2 in Fig. 3 then passes through heat exchangers present on the cold side of a heat pump described separately in section 3.2. At point 3 when sufficient heat has been removed from the primary air, it has become fully liquid with temperature T_3 and it can be stored at atmospheric pressure.

The secondary air stream also begins at high pressure and temperature T_1. This air is expanded isentropically to atmospheric pressure via the expander E_{sec} to yield a stream of cool air which passes through a heat exchanger, on the hotter side of the heat pump in order to draw heat from that heat pump.

At point 2', the secondary air is also at temperature T_2. The latent heat of evaporation of liquid air is very much larger than the total heat required to raise air from T_2 to T_1. Moreover, the heat discharged from a heat pump on its hotter side will necessarily be larger than the heat drawn in on its colder side. Thus, it becomes obvious that the secondary air stream will not provide enough capacity for heat removal from the heat exchanger if the amount of secondary air suggested by an exergy-balance is used directly for cooling.

The isothermal compressor, C_{iso}, shown in Fig. 3 between E_{pri} and E_{sec} provides one means by which the notional system can be made fully reversible. By drawing some of the shaft power produced by E_{sec} to drive C_{iso}, the total mass flow rate of cool ambient-pressure air exiting E_{sec} can be multiplied such that there is now sufficient thermal capacity to remove all heat from the heat pump with all air discharged being at ambient temperature.

The heat pump in this system has a rather interesting configuration. Temperatures on its hot side range from T_2 to T_1 – close to 200K for air that started at 50bar prior to expansion. By contrast, temperatures on its cool side range from just T_3 to T_2 – typically ~20K.

3.2. PRACTICAL IMPLEMENTATION OF THE HYBRID ENERGY STORE

The system, apart from the storage containments, is composed of compressors, expanders and heat exchangers (including two-stream and multi-stream contra-flow).

Some assumptions for the analyses carried out in this paper are listed in Table 2.

Table 2: Assumptions for the analyses of forward and reverse conversion processes

Ambient temperature	290K
Ambient pressure	1atm
Pressure of air in compressed air store	50bar
Mass flow rate of primary air	1kg/s
Isentropic efficiency of air expanders	97%
Isentropic efficiency of refrigerant expanders	97%
Isentropic efficiency of refrigerant compressor	95%
Efficiency of near-isothermal compressor	90%
Compressed air to electricity conversion efficiency (or vice versa)	85%

An iterative procedure was devised to model the forward and reverse conversion processes. Key "residuals" – difference between the two sides of an equation that is to be solved – were identified based on the governing equations for heat exchanger units and compressors/expanders. The Newton-Raphson method was then employed which iteratively finds closer approximations to the roots of the governing equations and thus reduces the residuals towards zero.

The properties of air used in this study were calculated based on the mixture model of Lemmon *et al.* [40] which is explicit in Helmholtz energy. Ideal hydrogen was considered to be the refrigerant, and its properties were calculated from Leachman *et al.* [41]. The transport properties of air were calculated from Lemmon and Jacobsen [42], and the transport properties of hydrogen were calculated from Assael *et al.*[43]

3.2.1. FORWARD CONVERSION PROCESS

The system for the conversion of high pressure (HP) air to liquid air is shown in Fig. 4. It comprises – in addition to an air-to-air pre-cooler for secondary air which reduces the work output after multi-stage expansion – a refrigerant compressor, sets of refrigerant expanders, and a pre-cooler for primary air. The refrigerant is compressed, and exchanges heat with multiple streams of secondary air

at the top of the heat pump (as depicted). After a single stage expansion in $E_{ref,1}$, the refrigerant expands in multiple stages (of equal pressure ratios) in $E_{ref,2}$ followed by successive reheats. In order to simplify presentation in Fig. 4, a convention is adopted to represent a collection of different items. The abbreviation *MEHXp* is employed to mean a provision comprising *multistage expansion with heat exchangers in parallel*. Fig. 5 clarifies this concept. In the present application, a single heat exchanger would have one fluid path carrying primary air (or refrigerant) at atmospheric pressure and *N* other fluid paths carrying the working fluid of the heat pump (or secondary air) at different pressures but spanning a similar range of temperatures. Thus, two *MEHXp* units have been considered – one with multiple refrigerant streams for exchanging heat associated with phase change of air (towards the bottom of the diagram in Fig. 4), and the other with multiple secondary air streams for exchanging heat associated with the compressed refrigerant at the top section Fig. 4.

A single *MEHXp* set operating with an ideal gas as the fluid being expanded (in equal pressure ratios) has a temperature ratio across the heat exchanger of:

$$\frac{T_{out}}{T_{in}} = \left(R_p\right)^{N(\gamma-1)/\gamma} \tag{2}$$

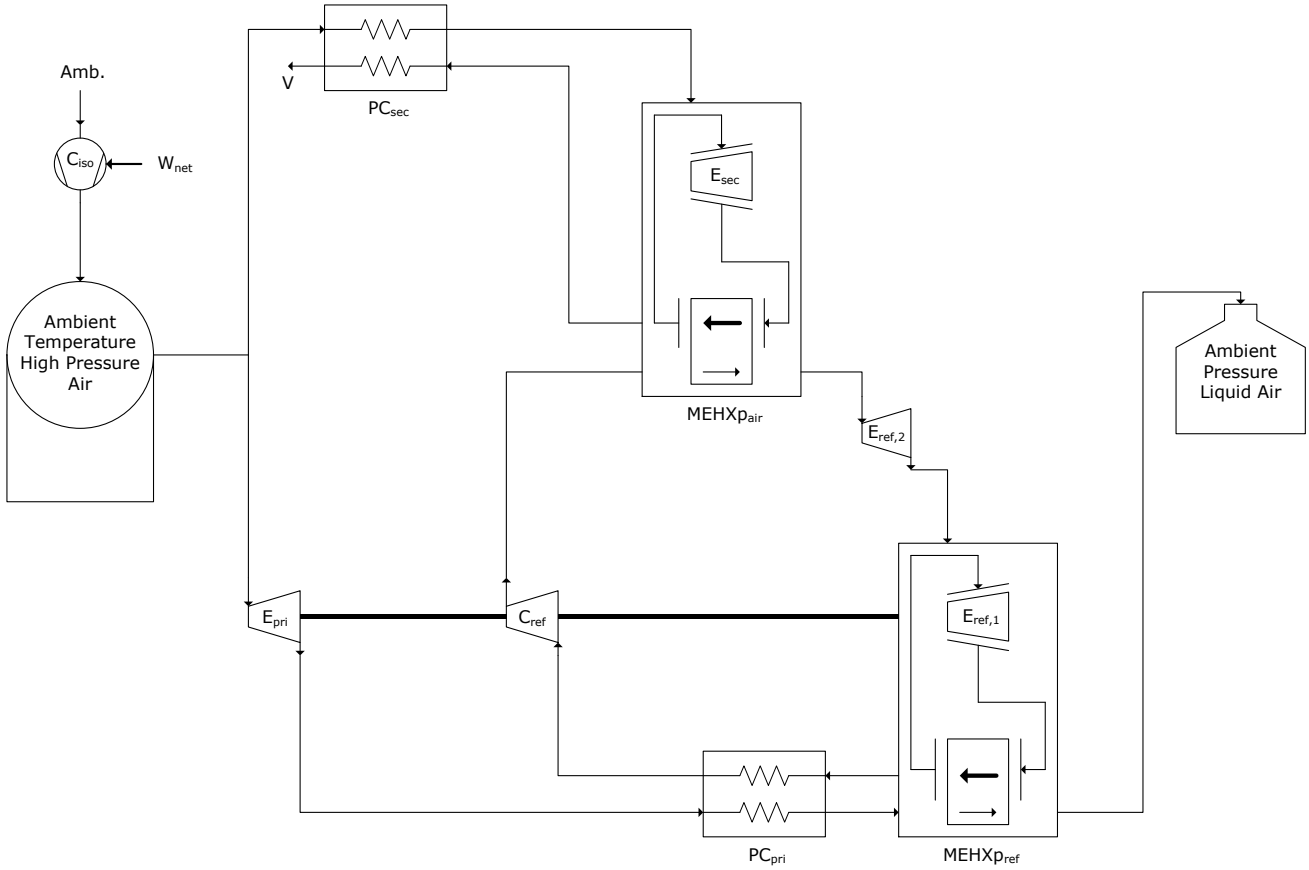

Figure 4: The forward conversion system for the hybrid energy store.

For the heat-exchange element of a single *MEHXp* set to be thermodynamically reversible, one requirement is that the specific heat, C_p, of the working fluid being expanded should be independent of pressure. We will assume this. It is also necessary that the variation of this C_p with temperature should be in proportion to the variation of C_p with temperature for the other fluid. This cannot generally be achieved exactly but by deploying several *MEHXp* sets in series, one may approach full reversibility arbitrarily closely.

As regards the compressor/expander, it can be particularly advantageous in terms of savings in capital costs if positive displacement machines are used, as the same machines can then operate in the reverse direction provided the number of stages in the compressor/expander remains the same.

The heat exchanger model in this work is based on the rating problem, i.e. by selecting the type of heat exchanger the performance (a measure of efficiency based on exergy) is evaluated.

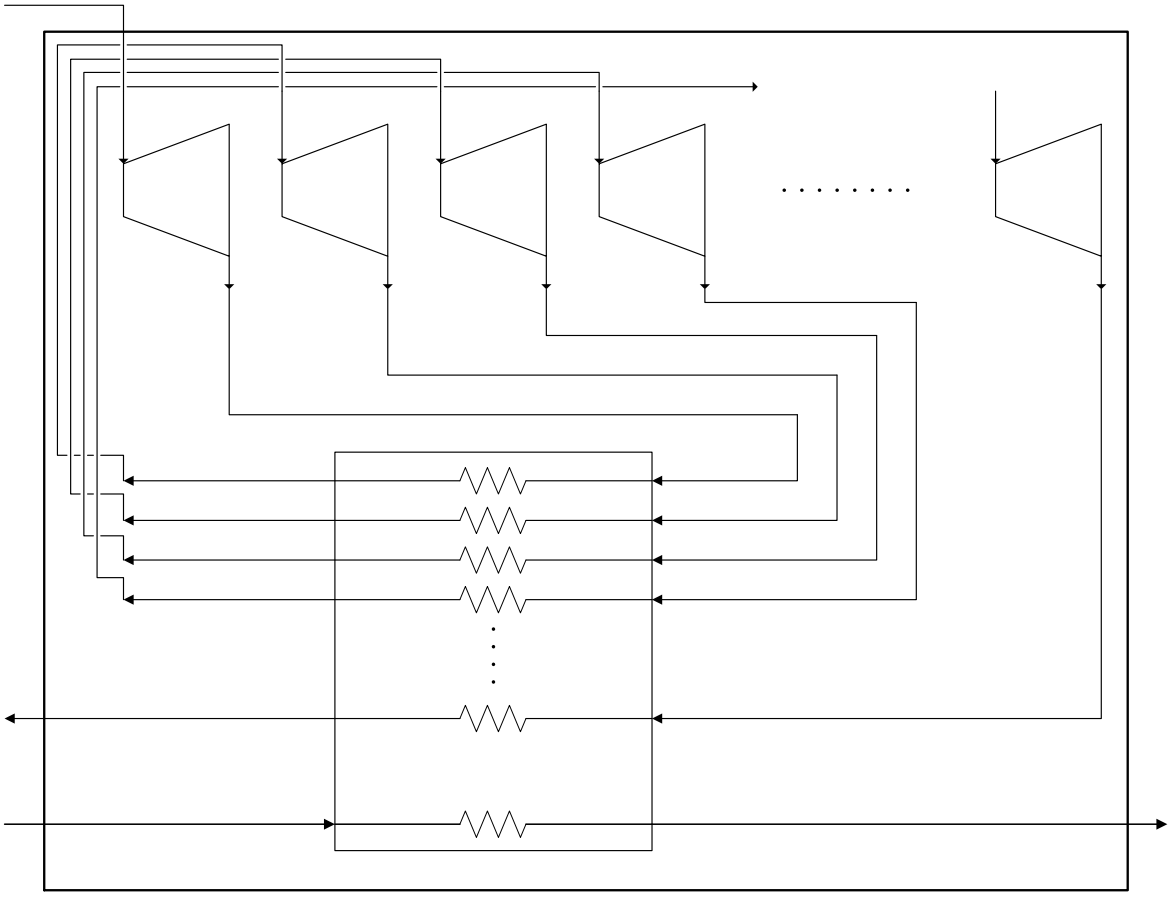

Figure 5: An *MEHXp* unit with *N* streams of one fluid exchanging heat with 1 stream of another fluid.

A two-stream contra flow heat exchanger of the finned shell-and-tube type is used for the secondary air precooler. The advantage here is the unit's ability to handle high pressures (of secondary compressed air). The primary air stream has a relatively high heat content associated with its transition from the gaseous phase to the liquid phase in the *MEHXp* unit at the bottom of the heat pump system in Fig. 4. Compact heat exchangers, like plate-fin type, spiral wound, and multi-pass shell and tube heat exchangers [44], which can also handle multiple streams, are commonly employed in cryogenic processes or when there is a need for highly effective heat exchange. Thus, multi-stream heat exchangers typically involve a large amount of heat transfer with small approach temperatures – where approach temperature is defined as the difference between outlet temperature of one stream and inlet temperature of the other stream – which enhances their efficiency [45]. Here, plate-fin type heat exchangers with offset fins are employed for the two-stream primary air-to-refrigerant heat exchanger, the refrigerant *MEHXp* unit (towards the bottom of Fig. 4), and the secondary air *MEHXp*

unit (towards the top of Fig. 4). It is assumed that: (a) the heat exchanger units operate in steady-state, (b) the pressure drop in the pipe work and heat exchanger units is negligible, (c) axial heat conduction in the heat exchangers is negligible, and (d) there is no fouling in the heat exchangers.

The governing equations for components involved in the system are listed below.

Expander model:

$$T_{out} = T_{in} + \eta_{s,exp}\left(T_{out,s} - T_{in}\right) \tag{3}$$

Compressor model:

$$T_{out} = T_{in} + \frac{\left(T_{out,s} - T_{in}\right)}{\eta_{s,comp}} \tag{4}$$

where,

$$T_{out,s,ref} = T_{in,H2}\left(\frac{P_{in,ref}}{P_{out,ref}}\right)^{(1-\gamma)/\gamma} \tag{5}$$

$$T_{out,s,air} = f\left(P_{in,air}, P_{out,air}, \rho_{out,air}, s_{in,air}\right) \tag{6}$$

Heat exchanger model:

An energy balance is applied for the heat exchangers, involving the calculation of three separate quantities, $\dot{Q}_{ref}$, $\dot{Q}_{air}$, and $\dot{Q}_{UA}$, where:

$$\dot{Q}_{UA} = UA\Delta T_m \tag{7}$$

$$\dot{Q}_{air} = \dot{m}_{air}\Delta h_{air} \tag{8}$$

$$\dot{Q}_{ref} = \dot{m}_{ref}\Delta h_{ref} \quad (9)$$

Where:

$$h_{ref} = C_{p,ref}T - C_{v,ref}T_0 \quad (10)$$

$$h_{air} = f(P, \rho, T) \quad (11)$$

The model holds when $\dot{Q}_{ref}$, $\dot{Q}_{air}$, and $\dot{Q}_{UA}$ (determined using equations (7), (8), and (9) respectively) are all equal.

The calculation of overall thermal conductance, *UA*, between the two streams requires the calculation of the heat transfer coefficients of both the air and the refrigerant stream(s). First we determine the heat transfer coefficient [46]

$$\alpha = JGC_p Pr^{-2/3} \quad (12)$$

J, the Colburn factor is given by [47]:

$$J = 2.11497 \times 10^{-2} - 1.02089 \times 10^{-5} Re + 2.37311 \times 10^{-9} Re^2 - 1.89734 \times 10^{-13} Re^3 \quad (13)$$

Where *Re* is given by:

$$Re = \frac{GD_h}{\mu} \quad (14)$$

Thus, *UA* is calculated using [46]:

$$\frac{1}{UA} = \frac{1}{(\eta_o \alpha A)_{air}} + \frac{1}{(\eta_o \alpha A)_{ref}} + R_w \quad (15)$$

Where the effectiveness of the finned surface, η_o, is given by [46]:

$$\eta_o = 1 - \frac{A_f(1 - \eta_f)}{A} \quad (16)$$

And the fin efficiency, η_f, is given by [46]:

$$\eta_f = \frac{\tanh(ml)}{ml} \tag{17}$$

If the stream of air undergoes phase change, the heat transfer coefficient is given by [48]:

$$\alpha = 1.06\left(\frac{{k_l}^3 {\rho_l}^2 g \Delta H_{2p}}{L_1 \mu_l \Delta T_{2p}}\right)^{1/4}\left(\frac{L_1}{D_h}\right)^{1/8} \tag{18}$$

The film to wall temperature difference, ΔT_{2p}, is given by:

$$\Delta T_{2p} = T_{air,m} - T_w \tag{19}$$

And the wall temperature, T_w, is given by [49]:

$$T_w = T_{air,m} + \frac{\left(T_{air,m} - T_{ref,m}\right)}{1 + \frac{(\alpha A)_{air}}{(\alpha A)_{ref}}} \tag{20}$$

The two-phase density, enthalpy and entropy are obtained by applying the linear rule of mixtures:

$$\rho_{2p} = x\rho_l + y\rho_v \tag{21}$$

$$h_{2p} = xh_l + yh_v \tag{22}$$

$$s_{2p} = xs_l + ys_v \tag{23}$$

With:

$$y = 1 - x \tag{24}$$

The liquid and vapour fractions and the corresponding densities of the liquid and vapour components are obtained by performing flash calculations by employing the SRK equation of state – details of this set of liquid-vapour equilibrium calculations for a mixture can be found in Ref. [50]

It becomes obvious that in order to obtain a two-phase heat transfer coefficient value from equation (18), an iterative procedure has to be employed.

The heat exchanger is split into many different sections along its length and the above calculations are performed for each section. Other calculations such as heat transfer areas and various other geometry relations for finned shell and tube heat exchangers as well as plate-fin heat exchangers with offset strip fins are provided in the appendix.

The mass flow rates and the number of stages can be varied to balance the (effective) $(\dot{m}C_p)$'s of the two fluids, thereby minimising exergy losses in the heat exchanger unit. The iterative method solves for unknown temperatures in the system, given the mass flow rates of secondary air and refrigerant, pressure at either the top-section or the bottom-section of the heat pump, compression ratio of C_{ref}, expansion ratio of $E_{ref,1}$, and the number of stages in E_{sec} and $E_{ref,2}$, which are listed in Table 3.

The secondary air stream is precooled in PC_{sec} before expansion in E_{sec}. To avoid this stream of air from being liquefied upon expansion, the number of expansion stages here was chosen to be two. The mass flow rate of secondary air was chosen such that the temperature of primary air after liquefaction would end up below bubble point temperature at ambient pressure. The mass flow rate of the refrigerant and the number of stages in the refrigerant *MEHXp* were chosen such that (a) the refrigerant would provide enough cooling capacity for the air stream being liquefied, and (b) exergy loss in the multistream heat exchanger is relatively low.

Table 3: Additional system parameters for the forward conversion process

Pressure at the top-section of the heat pump	60bar
Compression ratio of C_{ref}	6
Expansion ratio of $E_{ref,2}$	3.75
Mass flow rate of secondary air	3.6kg/s
Mass flow rate of refrigerant	0.9kg/s
Number of stages in $MEHX_{p,air}$	2
Number of stages in $MEHX_{p,ref}$	2

Tables 4a and 4b summarise the performance of the forward conversion process and list the distribution of exergy loss as a percentage of net flow exergy in. Any excess shaft power is used to drive a near-isothermal air compressor C_{iso} to suck in air from ambient and generate some feedback

flow exergy of compressed air. Thus, the exergy efficiency and the forward conversion efficiency are calculated as:

$$\eta_{ex,F} = \frac{\dot{B}_{LA} + \dot{W}_{net,out}}{\dot{B}_{CA}} \tag{25}$$

$$\eta_{c,F} = \frac{\dot{B}_{LA}}{\dot{B}_{CA} - \left(\eta_{elec,CA} \times \dot{W}_{net,out}\right)} \tag{26}$$

Table 4a: Performance summary of the forward conversion process using compressed air at a pressure of 50bar

Temperature of liquid air	77K
Exergy efficiency ($\eta_{ex,F}$)	71%
Forward conversion efficiency ($\eta_{c,F}$)	62%

Table 4b: Exergy loss distribution

Machine	**Fraction of net flow exergy in**
Primary air expander (E_{pri})	1.2%
Secondary air expanders (E_{sec})	3.4%
Refrigerant expander ($E_{ref,2}$)	3.6%
Refrigerant expanders ($E_{ref,1}$)	1.0%
Refrigerant compressor (C_{ref})	4.6%
Primary air pre-cooler (PC_{pri})	0.3%
Secondary air pre-cooler (PC_{sec})	3.2%
HXU connected with $MEHXp_{air}$	5.6%
HXU connected with $MEHXp_{ref}$	3.3%
Near-isothermal air compressor (C_{iso})	2.2%
Vent loss (V)	0.1%

Figs. 6(a)-6(d) show the temperature distribution along the lengths of the heat exchangers for the forward process. Hot secondary air at 50bar enters PC_{sec} at 290K and leaves the heat exchanger at a temperature just below 200K, whilst cool secondary air at ambient pressure enters PC_{sec} at ~170K and is vented to the atmosphere at a temperature just below ambient (Fig. 6(a)). Secondary air then expands in two stages with successive reheating, whilst cooling down the refrigerant from ~175K to ~120K (Fig. 6(b)). Meanwhile, the primary air stream after expansion in E_{pri}, is precooled in PC_{pri} from ~99K to a temperature just below its dew point at ambient pressure (Fig. 6(c)). It is then further

cooled to a temperature just below its bubble point at ambient pressure in $MEHXp_{ref}$, by two streams of refrigerant which undergo expansion and successive reheats similar to the secondary air stream in $MEHXp_{air}$ (Fig. 6(d)). The temperature of the primary air stream after liquefaction is ~77K.

Three sections were considered for each of the heat exchangers where there is no phase change, i.e. PC_{sec}, PC_{pri}, and $MEHXp_{air}$. It was found that at least three sections were needed in the heat exchanger where air undergoes phase change to capture the nonlinearities; five sections are considered in this work.

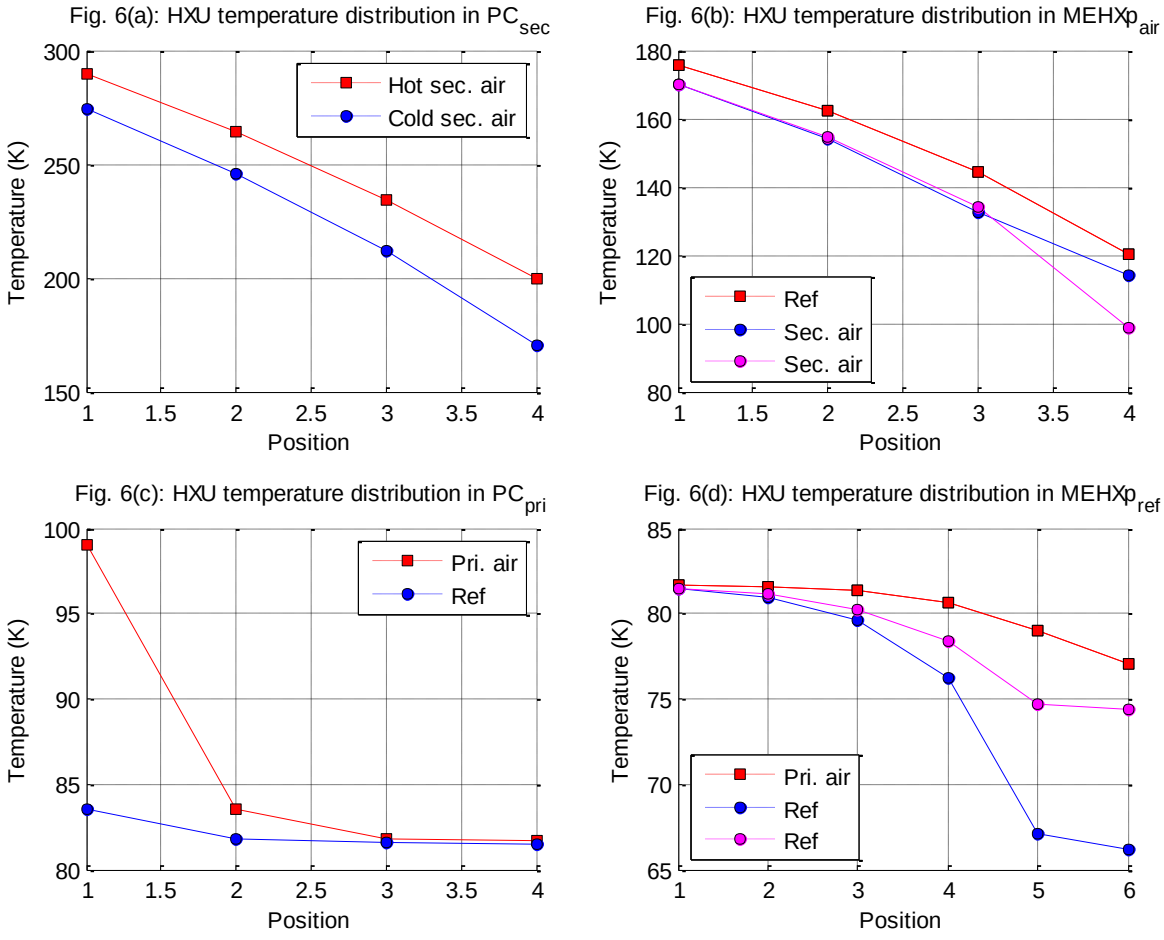

Figure 6: Variation of temperature along the length of the heat exchanger for the forward process.

3.2.2. REVERSE CONVERSION PROCESS

In the reverse conversion process, the flow directions of all fluids are reversed (Fig. 7). Hence the *MEHXp* units now function as *MCHXp* units, where the abbreviation means *multistage compression with heat exchanger units in parallel*. Air from ambient is drawn in by the first of the multiple secondary air compressors, first passing through the secondary air after-heater on its way into the compressor. The multiple streams of secondary air reject heat into the refrigerant stream at the upper-section of the heat engine, which in effect provides the heating capacity for the transition of liquid air to cool, gaseous air at the lower-section of the heat engine.

In the forward conversion process, the primary air stream is cooled down to about 77K at ambient pressure and stored in a well-insulated tank. If liquid air is stored in tanks with good thermal insulation, the losses can be quite low (0.05% by volume/day [51]). We will assume a non-negligible loss, and that the air rises up to a temperature just above its bubble point temperature before the reverse conversion process begins. Since, out of the two main diatomic components in air, nitrogen has the lower boiling point, the liquid will be richer in oxygen.

The system parameters specific to the analysis of the reverse conversion process are listed in Table 5, and the results in Tables 6a and 6b.

Table 5: Additional system parameters for the reverse conversion process

Pressure at the top-section of the heat pump	60bar
Expansion ratio of E_{ref}	6
Compression ratio of $C_{ref,2}$	3.75
Mass flow rate of secondary air	1kg/s
Mass flow rate of refrigerant	0.2kg/s
Number of stages in $MCHX_{p,air}$	2
Number of stages in $MCHX_{p,ref}$	2

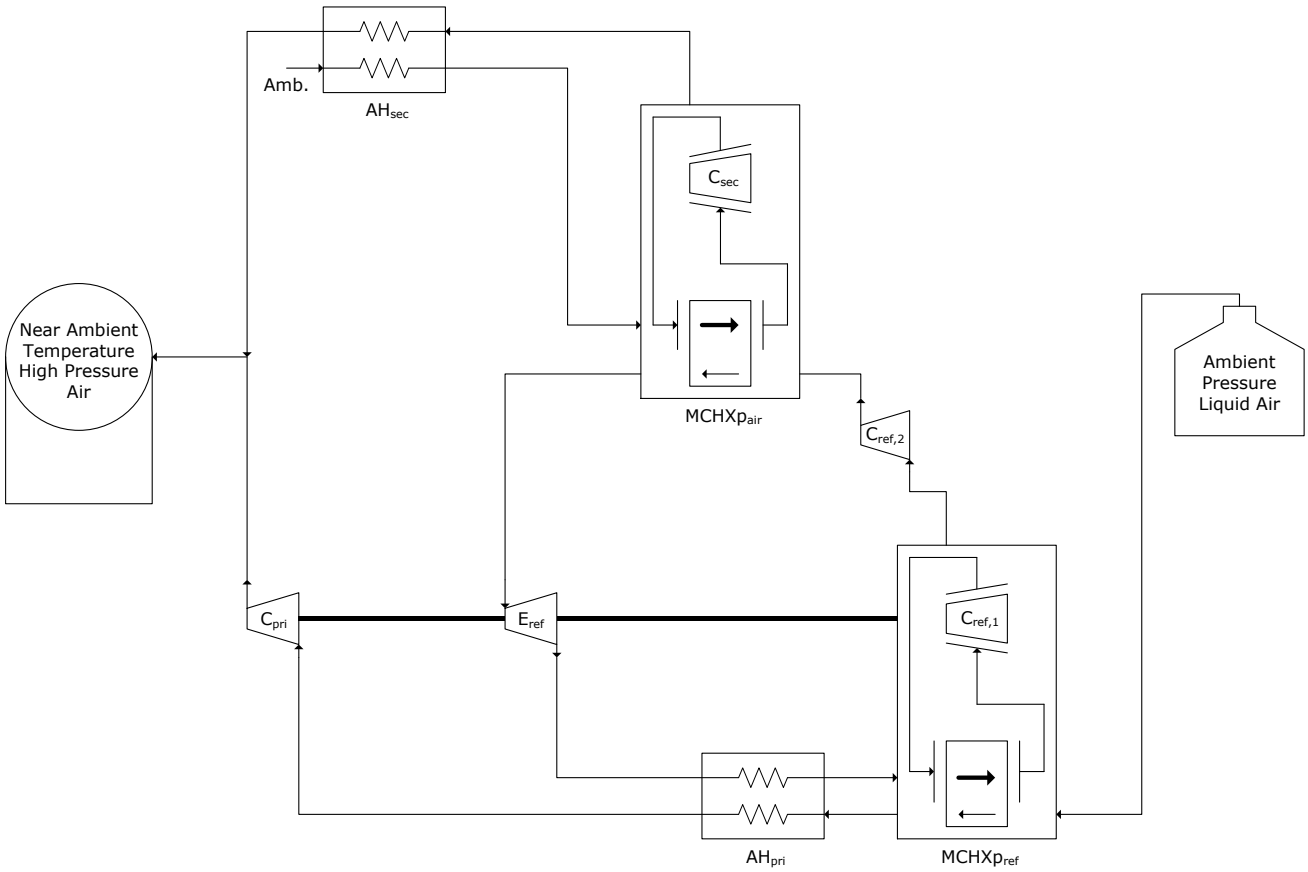

Figure 7: The reverse conversion system for the hybrid energy store.

The exergy efficiency and the reverse conversion efficiency are calculated as:

$$\eta_{ex,R} = \frac{\dot{B}_{CA}}{\dot{B}_{LA} + \dot{W}_{net,in}} \tag{27}$$

$$\eta_{c,R} = \frac{\dot{B}_{CA}}{\dot{B}_{LA} + \frac{\dot{W}_{net,in}}{\eta_{c,F}}} \tag{28}$$

Table 6a: Performance summary of the reverse conversion process resulting in compressed air at a pressure of 50bar

Temperature of compressed air in store	282K
Exergy efficiency ($\eta_{ex,R}$)	79%
Reverse conversion efficiency ($\eta_{c,R}$)	67%

Table 6b: Exergy loss distribution

Machine	Fraction of net flow exergy in
Primary air compressor (C_{pri})	0.7%
Secondary air compressors (C_{sec})	0.9%
Refrigerant compressor ($C_{ref,2}$)	0.7%
Refrigerant compressors ($C_{ref,1}$)	0.7%
Refrigerant expander (E_{ref})	2.3%
Primary air after-heater (AH_{pri})	6.7%
Secondary air after-heater (AH_{sec})	0.1%
HXU connected with $MCHXp_{air}$	8.7%
HXU connected with $MCHXp_{ref}$	0.6%

4. CONCLUSIONS

A novel hybrid energy storage system, comprising a compressed air store supplemented with a liquid air store of relatively higher energy storage capacity, is proposed. CAES offers high roundtrip efficiency, but aboveground storage of compressed air in a pressurised steel tank has significant costs associated with it. Liquid air energy storage on the other hand is not geographically constrained. It does not need a pressurised vessel for storage, but a very well thermally insulated container, which facilitates the storage of the cryogen for many months with negligible heat loss. Surplus shaft power output is used to convert compressed air at ambient temperature in the already nearly-full compressed air store to liquid air (the forward conversion process), and during times of high demand, liquid air is converted back to compressed air at near-ambient temperature, and the contained energy is then converted to electricity and sold to the grid. In this paper, detailed thermodynamic analyses of both the conversion processes have been carried out. The system is arranged in such a way that energy transactions with the grid are via the compressed air store since there may be times when it is not necessary to use the backup (liquid air) store and CAES can achieve higher roundtrip efficiencies (as air is compressed in the liquefaction process). Liquid air is obtained at ambient pressure. The secondary air takes away the heat rejected by the cooling system in the forward process, and is vented to the atmosphere at ambient pressure and near-ambient temperature. In the reverse process, both the primary air and secondary air streams are cooled and compressed to the desired pressure such that the final temperature of the air is close to ambient. For the conversion of HP air into liquid air (forward process), conversion efficiency is 63% if starting with 50bar HP air; the conversion process of liquid air into HP air at 50bar (reverse process) has efficiency of 67%.

Economic analysis of hybrid energy storage systems carried out in a separate study [15] shows that a hybrid CA-LA energy storage plant has the potential to provide greater ROI than the equivalent LAES plant, and greater ROI than the equivalent CAES plant if charge times are greater than about 36 hours. Although the hybrid plant has a relatively low roundtrip efficiency, it is somewhat redeemed by the fact that 10% of the total storage capacity is CAES; when used in isolation, the compressed air store has a much higher roundtrip efficiency than that obtained when the energy also passes through the liquid air store. The increased profits outweigh the slight increase in total plant cost.

APPENDIX

A. Geometry relations for finned shell and tube heat exchanger

In order to calculate the total heat transfer area the following parameters (Fig. A1) should be known a priori [52]: the length of the tube, L_1, the number of fins, N_f, the wall thickness of the tube, t_{wi}, the inner diameter of the tube, d_i, the inner diameter of the shell, D_i, and the fin thickness, δ.

The height of the fin is given by:

$$b = \frac{(D_i - d_o)}{2} \tag{29}$$

Where the outer diameter of the tube, d_o is given by:

$$d_o = d_i + 2t_{wi} \tag{30}$$

The hydraulic diameter is given by:

$$D_h = \frac{4A_o}{P_w} \tag{31}$$

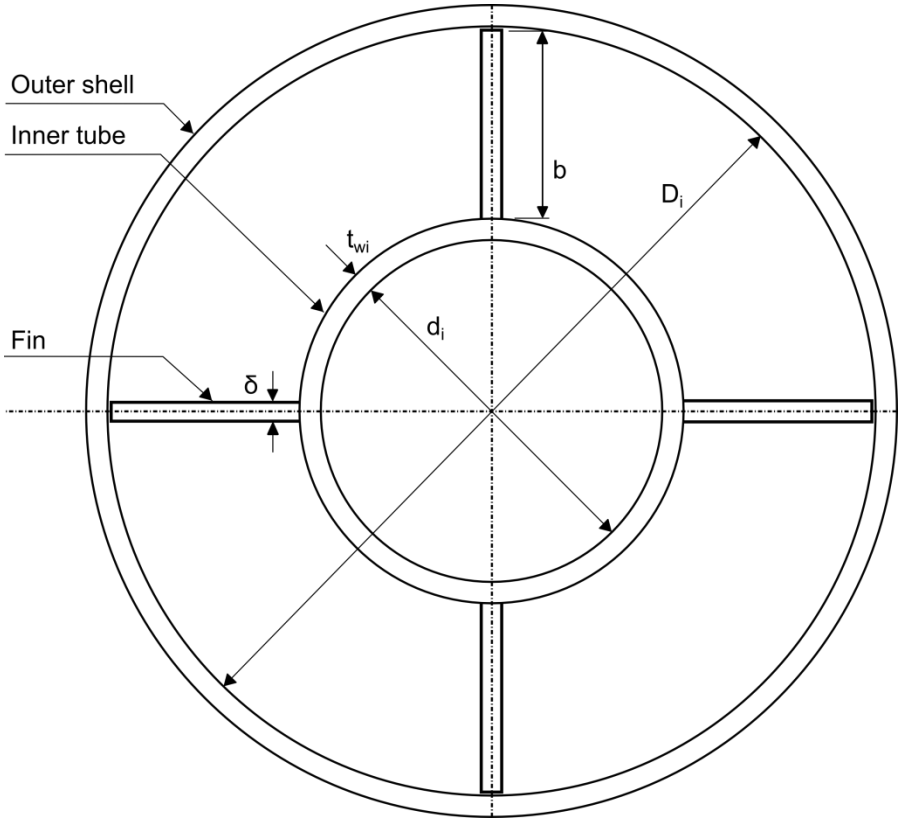

Figure A1: Cross-sectional view of a finned shell and tube heat exchanger of length L_1.

Where the freeflow area, A_o, between the shell and tube is given by:

$$A_o = \frac{\pi}{4}\left({D_i}^2 - {d_o}^2\right) - N_f b\delta \tag{32}$$

And A_o inside the tube is given by:

$$A_o = \frac{\pi {d_i}^2}{4} \tag{33}$$

Similarly, the wetted perimeter, P_w, for the shell is given by:

$$P_w = \pi(D_i + d_o) + 2N_f b - 2N_f \delta \tag{34}$$

And P_w for the tube is given by:

$$P_w = \pi d_i \tag{35}$$

The fin parameter, m, in equation (17) is given by:

$$m = \sqrt{\frac{2\alpha}{\delta k_f}} \tag{36}$$

And the fin length for heat conduction, l, in equation (17), is given by:

$$l = b \tag{37}$$

The wall resistance is given by:

$$R_w = \frac{\ln(d_o/d_i)}{2\pi k_w L_1} \tag{38}$$

The total heat transfer area, A, is the sum of the primary and secondary (fin) surface areas (A_p and A_f respectively), which are calculated as:

$$A_p = \pi d_o L_1 - N_f \delta L_1 \tag{39}$$

$$A_f = N_f L_1 (2b + \delta) \tag{40}$$

Thus, A is calculated as:

$$A = A_p + A_f \tag{41}$$

B. Geometry relations for plate-fin heat exchanger with offset strip fins

Here, the following parameters (Figs. B1-B2) should be known a priori in order to calculate the total area of heat transfer for a plate-fin heat exchanger with offset fins [46]: the length of the

plate, L_1, the width of the plate, L_2, the number of passages, N_p, the fin flow length, L_f, the fin pitch, p_f, the distance between interruptions, L_{eff}, the fin height, b, and the fin thickness, δ.

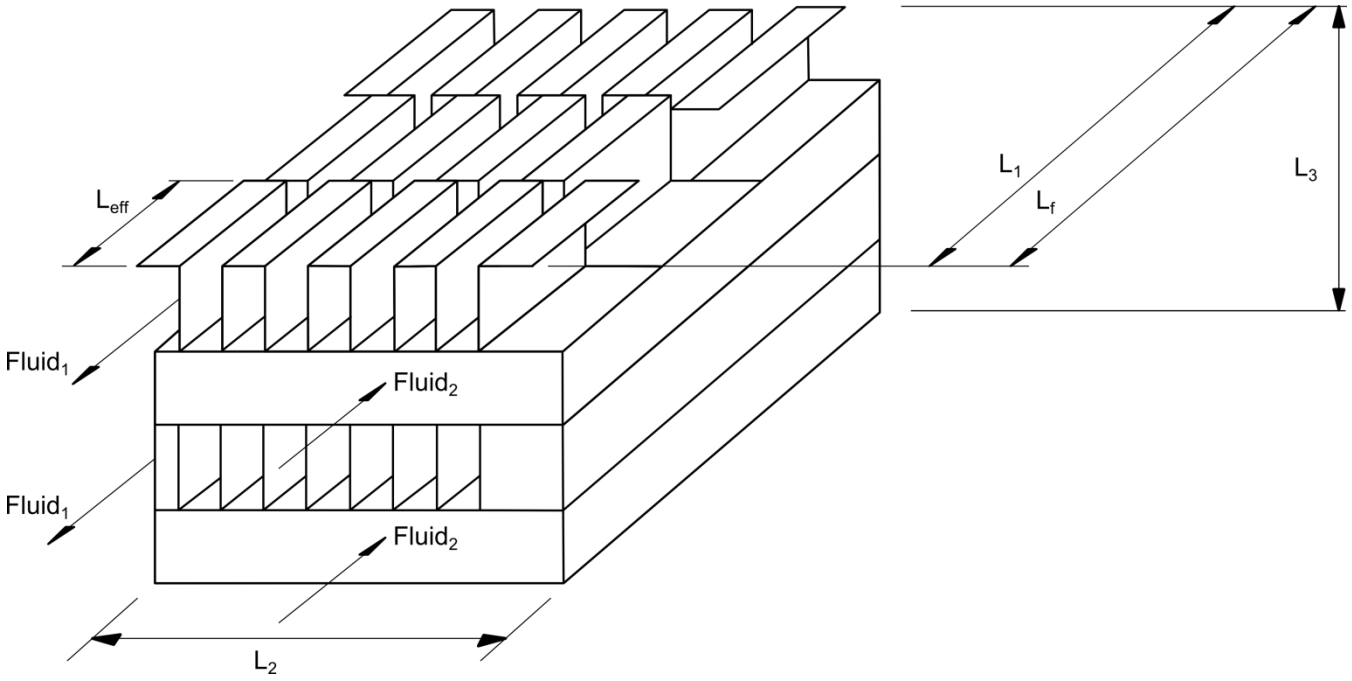

Figure B1: Plate-fin heat exchanger with offset strip fins.

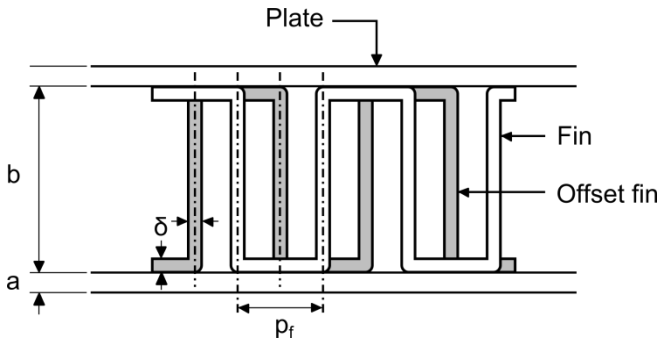

Figure B2: Idealised rectangular fin geometry for an offset plate fin heat exchanger.

The number of offset fins is given by:

$$N_{off} = \frac{L_f}{L_{eff}} \tag{42}$$

The number of fins is given by:

$$N_f = \frac{L_2}{p_f} \tag{43}$$

The hydraulic diameter is given by:

$$D_h = \frac{4A_o L_1}{A} \tag{44}$$

The wall resistance is given by:

$$R_w = \frac{a}{A_w k_w} \tag{45}$$

With:

$$A_w = L_1 L_2 N_{SP} \tag{46}$$

The fin parameter, m, is given by:

$$m = \sqrt{\frac{2\alpha}{\delta k_f}\left(1 + \frac{\delta}{\xi}\right)} \tag{47}$$

The freeflow area, A_o, is given by:

$$A_o = bL_2N_p - \left[(b - \delta) + p_f\right]\delta N_f \tag{48}$$

And the total heat transfer area, A, is given by the sum of primary surface area, A_p, and secondary (fin) surface area, A_f:

$$A_p = \left(2L_1L_2N_p - 2\delta L_f N_f\right) + \left(2bL_1N_p\right) + \left(2(b + 2a)\left(N_p + 1\right)L_2\right) \tag{49}$$

$$A_f = \left(2(b - \delta)L_f N_f\right) + \left(2(b - \delta)\delta N_{off} N_f\right) + \left(\left(p_f - \delta\right)\delta\left(N_{off} - 1\right)N_f + 2p_f\delta N_f\right) \tag{50}$$

$$A = A_p + A_f \tag{51}$$

REFERENCES

[1] REN21, "2013 Global Status Report," 2013. [Online]. Available: www.ren21.net. [Accessed 10 February 2014].

[2] Energy Research Partnership, "The future role for energy storage in the UK," 2011. [Online]. Available: www.energyresearchpartnership.org.uk. [Accessed 7 2014 March].

[3] Ridge Energy Storage, "CAES technology overview," [Online]. Available: www.ridgeenergystorage.com. [Accessed 3 June 2014].

[4] M. Swierczynski, R. Teodorescu, C. N. Rasmussen, P. Rodriguez and H. Vikelgaard, "Overview of the energy storage systems for wind power integration enhancement," in *Proceedings of the IEEE international symposium on industrial electronics*, 2010.

[5] P. Alotto, M. Guarnieri and F. Moro, "Redox flow batteries for the storage of renewable energy: a review," *Renewable and Sustainable Energy Reviewes,* vol. 29, pp. 325-335, 2014.

[6] S. van der Linder, "Bulk energy storage potential in the USA, current developments and future prospects," *Energy,* vol. 31, pp. 3446-3457, 2006.

[7] H. S. Chen, T. N. Cong, W. Yang, C. Q. Tan, Y. L. Li and Y. L. Ding, "Progress in electrical energy storage system: a critical review," *Progress in Natural Science,* vol. 19, pp. 291-312, 2009.

[8] P. Denholm, E. Ela, B. Kirby and M. Milligan, "The role of energy storage with renewable energy generation," NREL, 2010.

[9] D. Rastler, "Electricity Energy Storage Technology Options," 2010. [Online]. Available: www.epri.com. [Accessed 7 March 2014].

[10] J. N. Baker, "Electrical energy storage at the turn of the millennium," *Power Engineering Journal,* vol. 13, no. 3, p. 107, 1999.

[11] N. S. Wade, P. C. Taylor, P. D. Lang and P. R. Jones, "Evaluationg the benefits of an electrical energy storage system in a future smart grid," *Energy Policy,* vol. 38, no. 11, pp. 7180-7188, 2010.

[12] C. A. Ordonez, "Liquid nitrogen fueled, closed Brayton cycle cryogenic heat engine.," *Energy Conversion and Management,* vol. 41, no. 4, pp. 331-341, 2000.

[13] Centre for Low Carbon Futures 2050, "Liquid air in the energy and transport systems," The Centre for Low Carbon Futures, 2013.

[14] Y. Li, H. Chen, X. Zhang, C. Tan and Y. Ding, "Renewable energy carriers: Hydrogen or liquid air/nitrogen?," *Applied Thermal Engineering,* vol. 30, no. 14-15, p. 1985–1990, 2010.

[15] A. J. Pimm, S. D. Garvey and B. Kantharaj, "Economic analysis of a hybrid energy storage system based on liquid air and compressed air," *Energy economics (under consideration).*

[16] S. Knoke, "Compressed air energy storage, Handbook of energy storage for transmission or distribution applications," EPRI, Eckroad, S., ed., 2002.

[17] D. Steward, G. Saur, M. Penev and T. Ramsden, "Lifecycle Cost Analysis of Hydrogen Versus Other Technologies for Electricial Energy Storage," National Renewable Energy Laboratory, 2009.

[18] F. Crotogino, K.-U. Mohmeyer and R. Scharf, "Huntorf CAES: more than 20 years of successful operation," Solution Mining Research Institute, 2001.

[19] M. Nakhamkin, L. Anderson, D. Turpin, J. Howard, R. Meyer, R. Schainker, R. Pollak and B. Mehta, "First U.S. CAES plant initial startup and operation," in *Proceedings of the American Power Conference*, 1992.

[20] R. Leithner and L. Nielsen, "Modelling and dynamic simulation of an underground cavern for operation in an innovative compressed air energy storage plant," in *5th International conference on energy, environment, ecosystems and sustainable development*, 2009.

[21] A. J. Pimm, S. D. Garvey and M. de Jong, "Design and testing of energy bags for underwater compressed air energy storage," *Energy,* vol. 66, pp. 496-508, 2014.

[22] S. Zunft, C. Jakiel, M. Koller and C. Bullough, "Adiabatic compressed air energy storage for the grid integration of wind power," in *6th International workshop on large-scale integration of wind power and transmission networks for offshore windfarms*, 2006.

[23] C. Jakiel, S. Zunft and A. Nowi, "Adiabatic compressed air energy storage plants for efficient peak load power supply from wind energy: the European project AACAES," *International Journal of Energy Technologyand Policy,* vol. 5, no. 3, pp. 296-306, 2007.

[24] REW Power, "ADELE - Adiabatic Compressed Air Energy Storage For Electricity Supply," 2010. [Online]. Available: www.rwe.com. [Accessed 3 June 2014].

[25] N. Hartmann, O. Vohringer, C. Kruck and L. Eltrop, "Simulation and analysis of different adiabatic compressed air energy storage plant configurations," *Applied Energy,* vol. 93, pp. 541-548, 2012.

[26] F. D. S. Steta, "Modelling of an advanced adiabatic compressed air energy storage unit and an optimal model-based operation strategy for its integration into power markets," ETH Zurich, 2010.

[27] S. Freund, R. Schainker and R. Moreau, "Commercial concepts for adiabatic compressed air energy storage,"

in *7th International renewable energy storage conference*, 2012.

[28] "SustainX," [Online]. Available: http://www.sustainx.com/technology-isothermal-caes.htm. [Accessed 19 Nov 2014].

[29] "LightSail Energy," [Online]. Available: http://www.lightsail.com/. [Accessed 19 Nov 2014].

[30] C. A. Ordonez and M. C. Plummer, "Cold thermal storage and cryogenic heat engines for energy storage applications," *Energy Sources,* vol. 19, no. 4, pp. 389-396, 1997.

[31] A. Evans, V. Strezov and T. J. Evans, "Assessment of utility energy storage options for increased renewable energy penetration," *Renewable and Sustainable Energy Reviews,* vol. 16, pp. 4141-4147, 2012.

[32] R. Morgan, S. Nelmes, E. Gibson and G. Brett, "Liquid air energy storage - analysis and first results from a pilot scale demonstration plant," *Applied Energy,* vol. 137, pp. 845-853, 2015.

[33] E. M. Smith, "Storage of electrical energy using supercritical liquid air," in *Proceedings of IMechE*, 289-298, 1977.

[34] B. Ameel, C. T'Joen, K. De Kerpel, P. De Jaeger, H. Huisseune, M. Van Belleghem and M. De Paepe, "Thermodynamic analysis of energy storage with a liquid air Rankine cycle," *Applied Thermal Engineering,* vol. 52, pp. 130-140, 2013.

[35] Y. Li, H. Chen and Y. Ding, "Fundamentals and applications of cryogen as a thermal energy carrier: a critical assessment," *International Journal of Thermal Sciences,* vol. 49, no. 6, pp. 941-949, 2010.

[36] Y. Li, Y. Jin, H. Chen, C. Tan and D. Y., "An integrated system for thermal power generation, electricial energy storage and CO2 capture," *International Journal of Energy Research,* vol. 35, pp. 1158-1167, 2011.

[37] Y. Li, X. Wang and Y. Ding, "A cryogen-based peak shaving technology: systematic approach and techno-economic analysis," *International Journal of Energy Research,* vol. 37, pp. 547-557, 2013.

[38] J. Szargut, Exergy Method: Technical and Ecological Applications, WIT Press, 2005.

[39] L. Borel and D. Favrat, Thermodynamics and Energy Systems Analysis, Presses Polytechniques Universitaires Romandes#, 2010.

[40] E. W. Lemmon, R. T. Jacobsen, S. G. Penoncello and D. G. Friend, "Thermodynamic Properties of Air and Mixtures of Nitrogen, Argon, and Oxygen from 60 to 2000K at Pressures upto 2000MPa," *Journal of Physical and Chemical Reference Data,* vol. 29, p. 331, 2000.

[41] J. W. Leachman, R. T. Jacobsen, S. G. Penoncello and E. W. Lemmon, "Fundamental Equations of State for Parahydrogen, Normal Hydrogen, and Orthohydrogen," *Journal of Physical and Chemical Reference Data,* vol. 38, p. 721, 2009.

[42] E. W. Lemmon and R. T. Jacobsen, "Viscosity and thermal conductivity equations for nitrogen, oxygen,

argon, and air," *International Journal of Thermophysics,* vol. 25, no. 1, pp. 21-69, 2004.

[43] M. J. Assael, S. Mixafendi and W. A. Wakeham, "The viscosity and thermal conductivity of normal hydrogen in the limit of zero density," *Journal of Physical and Chemical Reference Data,* vol. 14, no. 4, pp. 1315-1324, 1986.

[44] M. M. Hasan, I. A. Karimi and H. E. Alfadala, "Modeling Phase Change in Heat Exchanger Network Synthesis," in *18th European Symposium on Computer Aided Process Engineering*, Lyon, 2008.

[45] T. M. Flynn, Cryogenic Engineering, 2nd ed., New York: Marcel Dekker, 2005.

[46] W. M. Rohsenow, J. P. Hartnett and E. N. Ganic, Handbook of heat transfer applications, McGraw Hill, 2nd ed., 1985.

[47] W. M. Kays and A. L. London, Compact heat exchangers, McGraw Hill, 2nd ed., 1964.

[48] J. W. Westwater, "Boiling heat transfer in compact and finned heat exchangers," in *Advances in two-phase flow and heat transfer*, Springer Netherlands, 1983, pp. 827-857.

[49] J. Taborek, Handbook of heat exchanger design, Hemisphere Publishing Corporation, 1984.

[50] J. M. Smith, H. C. Van Ness and M. M. Abbott, Introduction to Chemical Engineering Thermodynamics, McGraw-Hill, 7th ed., 2005.

[51] Y.-M. Yang, "Development of the world's largest above ground full containment LNG storage tank," in *23rd World gas conference*, 2006.

[52] S. Kakac, H. Liu and A. Pramuanjaroenkij, Heat exchangers: selection, rating and thermal design, CRC Press, 3rd ed., 2012.